Research Article

URF PUBLISHERS
connect with research world

Journal of Petroleum & Chemical Engineering

https://urfpublishers.com/journal/petrochemical-engineering

Vol: 1 & Iss: 1

High Efficient Photocatalytic Degradation of Formaldehyde Over Titania Photocatalyst Doped with Tungsten

Van Thi Thanh Ho[1]*, Quynh Le Nguyen Huong[2], Khuong Anh Nguyen Quoc[3], Bao Dinh Gia Pham[4], Tam Thi My Luu[4], Duy Nguyen Huynh Minh[4], Tuan Huynh Nguyen Anh[4]

[1]Institute of High Tech Training Victoria (Vitech)- Hoa Binh University, Vietnam

[2]Ho Chi Minh City University of Technology, VNU-HCM, Ho Chi Minh city, Vietnam

[3]NTT Institute of High Technology, Nguyen Tat Thanh University, Ho Chi Minh City, Vietnam

[4]Faculty of Chemical and Food Technology, University of Technology and Education, Ho Chi Minh city, Vietnam

Citation: Thanh Ho VT, Huong QLN, Quoc KAN, et al. High Efficient Photocatalytic Degradation of Formaldehyde Over Titania Photocatalyst Doped with Tungsten. *J Petro Chem Eng* 2023;1(1): 10-18.

Received: 20 October, 2023; **Accepted:** 24 October, 2023; **Published:** 05 November, 2023

***Corresponding author:** Van Thi Thanh Ho, Institute of High Tech Training Victoria (Vitech)- Hoa Binh University, VietNam, Email: httvan@hcmunre.edu.vn

Graphical Abstract

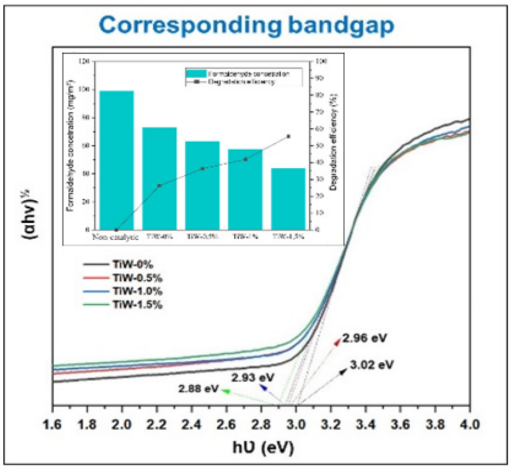

ABSTRACT

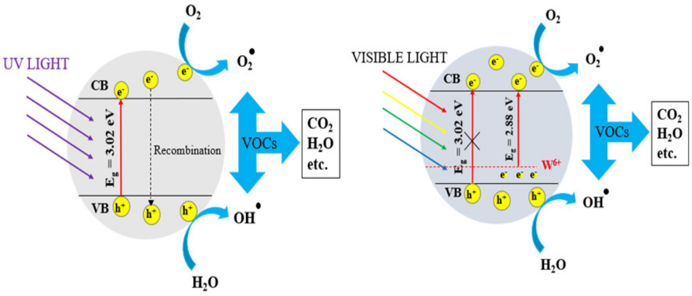

In recent developments in treating volatile organic compounds (VOCs), there has been growing interest in using metal-doped TiO2 photocatalysts. This approach offers a practical, easily implementable, highly catalytic, non-toxic, and cost-efficient method for treating pollutants. It addresses some of the limitations of pristine TiO2, including its wide bandgap and limited surface area. The present study focuses on the one-step, environmentally friendly synthesize of a W-doped TiO2 catalyst at 200°C for 10 hours, not using surfactants or post-reaction calcination. We systematically investigated the impact of different W doping ratios (0%, 0.5%, 1%, and 1.5%) on the catalyst's properties, yielding insightful outcomes. The resulting catalyst exhibited superior attributes, including an increased surface area of 175 m2/g, a uniform spherical morphology with particle sizes of 6 - 10 nm, and a reduced bandgap energy (2.88 eV). Notably, this catalyst demonstrated a feasible efficiency in VOCs treatment, achieving a decomposition efficiency of 71.98% for formaldehyde. Consequently, the facile solvothermal synthesize of W-doped TiO2 photocatalysts holds promise as a prospective strategy for gas processing applications in the future.

Keywords: W-doped TiO2, TiO2 based, photocatalyst, VOCs degradation, nanomaterial, photocatalytic activity

---

1. Introduction

The release of volatile organic compounds (VOCs) has had obvious negative consequences on people's health and the environment. They specifically induce a variety of symptoms such as headaches, dizziness, and irritability, and can even result in cancer and mutation[1]. This harmful emission is associated with the industrial manufacturing process, automobiles...[2,3]. There were numerous methods for eliminating VOCs from the air, including (i) biological filtration[4], (ii) oxidation[5,6], (iii) absorption[7,8], and (iv) adsorption[9]. However, there are various limitations such as high cost[9], necessitating interaction between VOCs and organisms[4], elevated temperature[6], or selective adsorption in wet conditions[10].

Until now, researchers have been interested in another method of treating VOCs - using photocatalysts, with TiO_2 being one of the signature examples. Masato *et al.* produced the TiO_2/Y-zeolite hybrid photocatalyst in 2012, which aids in the removal of aromatic chemicals such as toluene and benzene from the air phase[11]. Nataša Novak Tušar *et al.* created TiO_2 - SiO_2 films from organic-free colloidal TiO_2 anatase nanoparticles in 2016[12]. Scientists want to dope TiO_2 because it is an environmentally friendly photocatalyst with high catalytic activity, is non-toxic, durable, and cost-effective[13]. TiO_2 has three structural morphologies that correlate to anatase, rutile, and brookite. Brookite is difficult to prepare, hence there are few reports on it. Furthermore, it is less durable than rutile[14]. Anatase and rutile have tetrahedral crystal cells, with 1 Ti^{4+} bonded to 6 O^{2-} ions and 1 O^{2-} ion bound to 3 Ti^{4+} ions. The distinctions between these morphologies, including their electrical structure and optical characteristics, are due to variations in lattice structure[15]. Anatase is expected to have higher catalytic activity than rutile due to its larger band distance (3.2eV), longer electron lifetime as a photobiotic electron-hole[16], and better conduction band position[17]. Furthermore, the estimated average effective mass of electrons and smaller electron holes improve electron movement[16], and a larger surface area leads to improved photocatalytic effectiveness[17]. However, there are certain limits to TiO_2 applications, such as a large energy range (from 3.0 to 3.2 eV) that only operates in the UV light zone, and nano TiO_2 is prone to agglomeration[13]. The transition of TiO_2's optical response from the ultraviolet to the visible light zone will have a significant impact on the material's practical applicability[18]. Several research based on doping metals have been undertaken to reduce the band gap of TiO_2 materials, with the hope that metal ions can occupy the various positions on the TiO_2 surface. This method of improving photocatalytic capabilities has several advantages, including the formation of electron traps that inhibit electron and hole recombination, which increases VOCs adsorption to the material's surface due to changes in surface charge, and increased interaction with VOCs[18]. Wenjun Liang's research group used sol-gel methods to synthesize Ag/TiO_2 and Ce/TiO_2 materials in 2011, giving formaldehyde decomposition efficiencies of 87% and 90% respectively[19]. In 2017, Yaobin Li et al. developed Pd-doped TiO_2 capable of metabolizing formaldehyde at a concentration of 300 ppm for 30 hours with an 80% efficiency[20]. Baoqing Duan's team also successfully synthesized Zr-doped TiO_2 using the sol-gel method, yielding an amazing 83% formaldehyde treatment result[21].Studies on toluene processing are also of interest and are being carried out, such as the V-doped TiO_2/PU material with a band gap of 2.83 eV, with a toluene processing efficiency of 80% by the Byeong-Kyu Lee research group[22]. Many scholars throughout the world have also examined additional transition metals such as W, Fe, Cu, Mo, Mn, Zr, Ni and so on[23-29]. Not only metals but also nonmetallic elements are combined with TiO_2[30,31], forming composite materials[32,33] ...however, easy-to-form composite materials lack strength[34], and nonmetal-doped TiO_2 materials with low band energies are challenging to apply[35]. Although the option of doping metals into TiO_2 has many advantages, some study results are limited owing to the high band energy (> 3.0 eV), relatively low surface area (100 m^2/g) due to the use of sol-gel method performed at high temperature (~ 500°C)[30,36,37].

Tungsten doping has revealed numerous surprising novelties in investigations on doping metals into TiO_2 to tackle the aforementioned difficulties. The valence region of TiO_2 is primarily composed of 2p O states, whereas the conduction region mainly consists of 3d Ti, and for metal ions to be able to reduce recombination, a new energy level must be formed between these two bands[38]. Among metal ions, W^{6+} (r_W = 0.600 Å) has an ion radius similar to Ti^{4+} (r_{Ti} = 0.605Å), allowing for facile lattice substitution and the creation of a new band gap right below the semiconductor area[39,40]. At the same time, W-doped TiO_2 catalysis can benefit from the visible source due to the lowered band gap of 2.90 eV[23], since WO_3 has a band gap energy of roughly 2.5 eV[41] . In 2017, Ali's team used the sol-gel method to investigate the best conditions for treating toluene with synthetic W-modified TiO_2. At a concentration of 4000 ppm, the results showed that 0.52 wt.% W mass has the maximum efficiency, decomposing 59% more than the original. However, in this experiment, the optimum temperature for sample synthesize is up to 500°C[36]. $Ti_{0.7}W_{0.3}O_2$ material was successfully synthesized in 2018 using the solvothermal solution method from WCl_6 and $TiCl_4$. Hau Quoc Pham *et al.* discovered that 220°C and 4 hours were ideal circumstances and that the synthesized sample had a high specific surface area (approximately 127 m^2/g)[42]. In another work, $Ti_{0.7}W_{0.3}O_2$ did not exhibit a WO_3 peak in XRD analysis results after 10 hours at 200°C, and the synthesized sample had a significantly increased specific surface area (201.5 m^2/g)[43]. Even though these studies only looked at the effect of W-modifiers on electrochemical properties, the samples' conductivity improved significantly, implying that W^{6+} may have formed intermediate energy levels between the valence and conduction regions of TiO_2, which is required for metals to improve processing efficiency physics of photocatalysis.

In this paper, we suggest a single-step solvothermal solution approach for producing nanostructured W-doped TiO_2 photocatalysts for formaldehyde treatment. Our material is made here with no surfactants or other additives. The firing stage following the reaction simplifies the experimental process, reducing time, effort, and production costs. To boost catalytic activity, this approach was used to reduce particle size and increase the specific surface area of the photocatalyst material. Experiments with various low W ratios were also conducted to evaluate the impact on photodecomposition efficiency. As a result, we were able to successfully synthesize W-doped TiO_2 photocatalyst using a single-step solvothermal route, which promises good processing of volatile organic compounds and commercialization.

2. Methods

2.1 Chemicals

Tungsten (VI) chloride (CAS: 13283-01-7, $WCl_{6,}$ 99.9% trace metal basis) were original from Sigma-Aldrich, USA; Titanium tetrachloride (CAS: 7550-45-0, m = 500g, $TiCl_4$, 99.0%) were obtained from Aladdin, China; Ethanol absolute (CAS:64-17-5, C_2H_5OH, ACS reagent) were obtained from Merck, Germany; Formaldehyde (CAS: 50-00-0,HCHO, >95.0%, 500ml) came from Xilong Scientific, China; and Deionized water was utilized in all experiments.

2.2 Synthesizing photocatalyst W-doped TiO_2 materials

Tungsten-doped-TiO_2 material was prepared by one-step solvothermal route without any surfactants or stabilizers. The detailed steps are described in Figure 1:

Firstly, an identical amount of WCl_6 was dissolved in 50ml ethanol absolute to get the Tungsten's mole percentage of 0.5 mol%, 1 mol%, and 1.5 mol%, respectively and stirred for 20 mins. After becoming a homogeneous solution, the container was cooled in an ice bath while stirring consistently. Next, adding 0.55 mL $TiCl_4$ and putting the liquid solution above into a Teflon reaction sealed in an autoclave. The solvothermal reaction was conducted at 200^{0}C in 10h, cooling at room temperature. The sample was obtained after centrifugation, washing with Deionized water. At the end, the product was dried at 80^{0}C for further process.

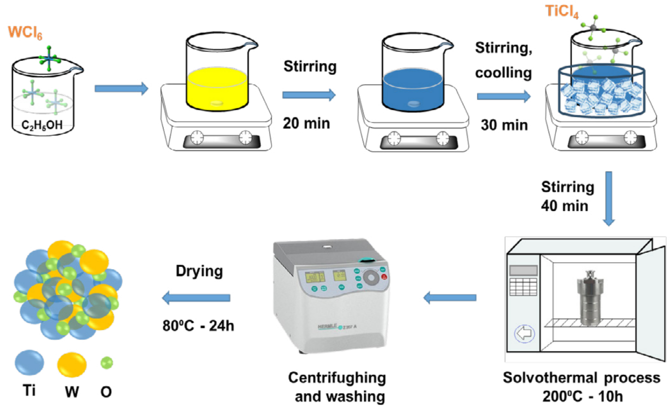

Figure 1 Synthesize process of TiW photocatalysis for VOCs treatment.

2.3 Sample Characterization

To determine the crystal structure of the material, Bruker D8 Advance X-ray diffractometer (XRD) with Cu Kα radiation (λ = 1.540598 nm) was utilized on the 2θ range of 10-70^o at a 5 min^{-1} scanning rate, dwell time 0.7 s/^{o}. The morphologies of the pure TiO_2 and W-doped TiO_2 samples were evaluated by transmission electron microscopy (TEM), filed emission scanning electron microscopy (SEM). The equipment used include: a JEM 1400 (JEOL Ltd., Tokyo, Japan) operated at 100kV, JSM-IT200 SEM (JEOL Ltd., Tokyo, Japan) …, respectively. X-ray fluorescence (XRF) measurement was applied on The model **XRF5006-**HQ02 VietSpace with a FAST SDD X-ray receiver, energy resolution of 135 eV, the X-ray emitter is the Oxford Inc. Series 5000. The sample is measured in a vacuum environment and processed digitally and calculated with an Amptek meter (USA). N_2 adsorption/ desorption isotherms in Brunauer-Emmett-Teller (BET) methods were evaluated in Surfer (KGW-ISOTHERM, Germany) to examine the pore size and surface area of W-doped TiO_2. The US-Visible diffuse reflectance spectra (DRS) of sample were conducted on UV-2600i (Shimadzu Ltd., Kyoto, Japan) combined with Integral ball IR-2600 Plus in the range from 220-1400 nm, halogen and deuterium lamp source, PMT R928 receiver. The gas samples are collected into the TEDLAR BAG 3L for formaldehyde concentration determination by GC/ECD-FID-TCD gas chromatographer. The concentration of VOCs present in the gas sample was analyzed for gas chromatography according to NIOSH METHOD 3500 for formaldehyde.

2.4 Formaldehyde Degradation Laboratory System

Figure 2 illustrates the experimental setup of the system used for the photocatalytic degradation tests. Formaldehyde concentrations were measured before and after the reaction. The first compressor (P1) pushed the air, which was subsequently filtered through two glass tubes. The first glass tube had silicates (3) in the middle to remove moisture from the air, while the second glass tube had activated carbon to purify the air and remove leftover moisture. To prevent air loss, they were both filled with glass wool (2) and sealed with a rubber cap (1). The stream was controlled using an F1 flow meter (F1). The sample drop (6), a combination of toluene and distilled water, was confined in a quartz tube (7) (5 mm in diameter). An alcohol burner (5) was located beneath the tube, evaporating the sample. The four-way cock was used to modify the stream's direction. To stabilize the concentration of inflow gas, toluene-containing air was pumped into a TEDLAR 3L air bag (9). The air from this air bag was then withdrawn using the second compressor (P2) for photocatalytic degradation. The F2 flow meter (F2) controlled the air flow before it passed through the photocatalyst layer as well as the duration for collecting reacted air. As a packed-bed reactor, a quartz tube (10) (100 mm length, 5 mm diameter) was filled with previously manufactured W-doped TiO_2 photocatalyst. As light sources, two identical UV lamps (12) (Ecomax, 25 W) with 132.6 W/m^2 irradiation power and a minimum wavelength of 255 nm were utilized. The fan (8) assisted in cooling these two bulbs. The reactive air was collected using another TEDLAR air bag (13) for further examination. The concentration of toluene in the input collected by bag (9) (C0) and the outlet collected by bag (13) (C) was then determined using gas chromatography (Agilent 6890 N Network Gas Chromatograph). Each experiment's efficiency (E) was then determined as follows: $E = 1 - CC0 \cdot 100\%$. Finally, the air was forced through a glass tube containing activated carbon to confirm that the exit gas was safe.

The experiments were applied in bellowing steps:

- Attach the inlet sample air collection bag to the position connected to valve V3, open valve V6 (valve of the airbag), adjust the flowmeter F1 to 1 L/min, lock all valves, stuff glass and drip sample (including 0.05 mL formaldehyde and V mL distilled water) to the sample droplet tube, Light an alcohol lamp and heat the glass tube containing the sample drop over the flame for 1 minute.

- Open valves V5 and V3, turn on pump P1 and start countdown timer, collect air within 3 minutes for air to fill the bag, lock the V6 airbag valve in turn, turn off the pump and alcohol lamp, lock the remaining valves. Attach the air bag to the connection position with valve V11, open valve V12 of the airbag.
- Stuff 0.1 grams of synthesized catalytic material into the glass tube, divide the amount of catalyst into 3 equal segments alternately with glass wool samples so that the catalyst is evenly distributed over the tube. Turn on the radiator fan, light, let the lamp operate for 10 minutes before operation to ensure the amount of radiation emitted is stable.
- Turn on compressor P2 with a fixed F2 flow rate of 300 mL/min and collect air for 10 minutes until the airbag (9) has no sample left. Lock valves V11, V12 and remove the airbag containing the air sample, then turn off P2, turn off the light.
- After the gas collection is completed, clean the system again, the glass tubes containing the sample drop and catalytic column, lock the V3 valve, open the V2 and V13 valves to blow air into the system cleaning, then lock all valves, prepare for the next experiment.
- The airbag containing the sample, after being labeled, is put into the tank and transferred to the analysis company for gas chromatography analysis to determine the concentration of formaldehyde.

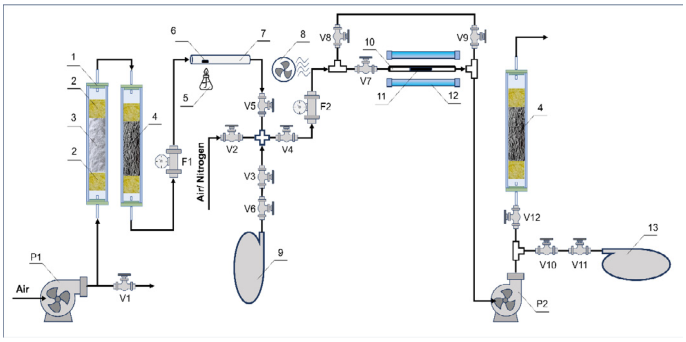

Figure 2: Schematic of formaldehyde degradation system. 1. Rubber cap; 2. Glass wool; 3. Silica gel; 4. Activated carbon; 5. Alcohol burner; 6. Drops of formaldehyde and water; 7. Quartz tube; 8. Cooling fan; 9. Sample gas inlet bag; 10. Catalyst tube; 11. Catalytic materials; 12. Light; 13. Sample gas storage bag; P1: Compressor; P2. Compressor; F1: Flow meter for inlet gas; F2: Flow meter for gas passing through photocatalyst layer.

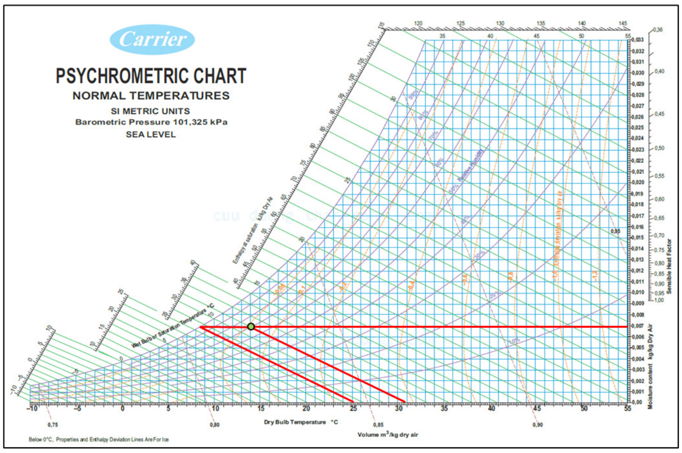

Figure 3: Psychrometric chart [44].

3. Results and Discussion

3.1 Results of analyzing the composition, morphology, and structure of the W-doped TiO_2 nano photocatalytic material

XRD patterns of TiO_2 and W-doped TiO_2 catalyst samples with different ratios are shown in Figure 4a XRD patterns show diffraction peaks recorded at positions 25.3°, 37.8°, 48.0°, 53.9°, 55.1°, 62.8°, corresponding to the (101), (004), (200), (105), (211) and (204) planes, showing the phase formation orientation of anatase TiO_2 (JCPDS - 84 - 1286). There was no formation of WO_3/TiO_2 composite because the characteristic diffraction peaks of WO_3 were not detected (JCPDS - 20 -1324) (at 2θ ~ 23.0°, 23.7°, 24.0°) showing that the creation of oxide impurities of W does not occur, thereby confirming the substitution of W into the structural framework of TiO_2. There is not much difference in the peak position of the W-doped TiO_2 material samples compared to TiO_2. This may be due to the negligible difference in radius between W^{6+} (0,600 Å) and Ti^{4+} (0,605 Å), and the doping percentage is not much. The high-intensity peaks show a higher tendency to form anatase phase than rutile, possibly due to the synthesize conditions of 200°C for 10 hours. At this condition, amorphous TiO_2 is completely transferred to the anatase, but not enough to convert the anatase to the rutile phase[14]. These results are also consistent with previous research[45]. Comparing W-doped TiO_2 samples, as the doping W content increases, the signal intensity decreases, and the peak width increases. This shows that W-doped TiO_2 has reduced the crystal size. The crystallite size of the catalyst samples was determined according to the Scherrer equation in Figure 4b. These results show that low W-doped TiO_2 material has an anatase phase-oriented crystal structure and a small crystal size, and is a potential photocatalytic material[46].

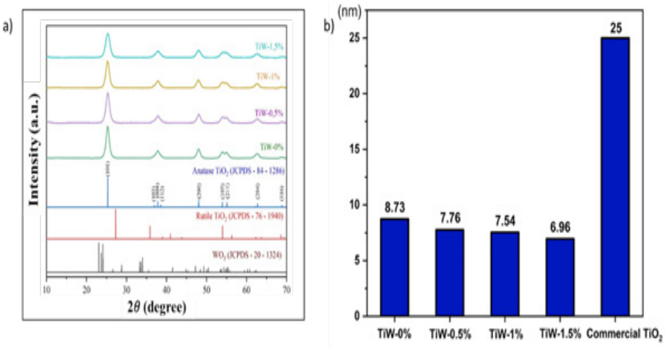

Figure 4: a) XRD patterns of pure TiO_2, TiW-0%, TiW-0.5%, TiW-1% and TiW-1.5%, b) Chart of crystallite size of various W ratios doped TiO_2.

Figure 5 displayed the distribution of elements O, Ti, W in the material. It can be seen that the elements are distributed quite evenly. The results of elemental ratio analysis from the XRF spectrum and Table 1 indicate that the ratio of W in the material also reaches a value close to the theoretical calculated value. This could be attributed to the preparation by solvothermal method with low temperature (200°C in 10 hours), which is a suitable and effective route.

Table 1: Percentage of Tungsten in different samples obtained from XRF analysis.

No.	Sample	Mol% of Tungsten
1	0.5 mol% W-doped	0.4%
2	1.0 mol% W-doped	1.3%
3	1.5 mol% W-doped	1.5%

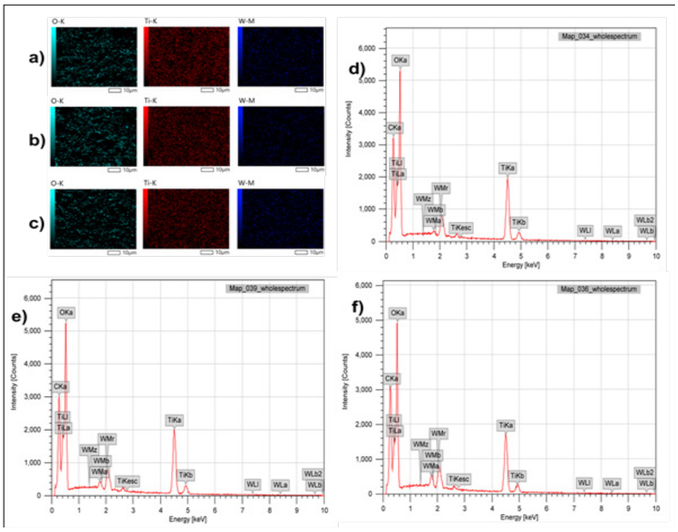

Figure 5: EDS analysis elemental mapping of a) TiW-0.5%, b) TiW-1%, c) TiW-1.5% and EDS spectra of d) TiW-0.5%, e) TiW-1%, f) TiW-1.5% samples.

The SEM images in Figure 6 show that the TiW-0% sample has the phenomenon of small particles agglomerating into blocks of unspecified size and shape. In W-doped TiO_2 samples, the particles tend to form spherical or near-spherical shapes. In addition, as the amount of W – doped increases, the agglomeration tends to decrease. With 1.5 mol% W-doped on TiO_2, the agglomeration recorded was the lowest, showing that the catalyst particles were distributed uniformly.

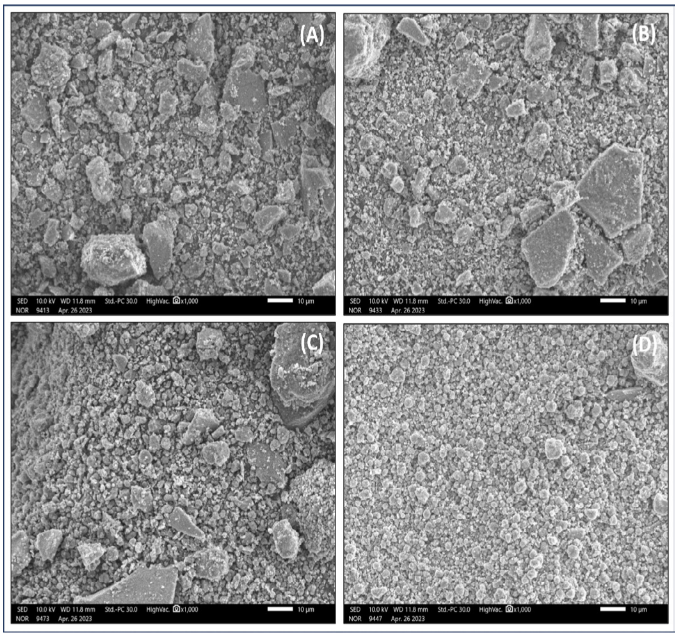

Figure 6: SEM images of a) TiW-0%, b) TiW-0.5%, c) TiW-1.0%, d) TiW-1.5%.

The HRTEM results of Figure 7 further confirm the uniform distribution of the W-doped TiO_2 material. In addition, these results indicate that the 1.5 mol% W-doped TiO_2 material has a particle size mainly between 6-10 nm. The particle size matches the crystallite size obtained from the XRD patterns.

N_2 adsorption and desorption methods determined the specific surface area and pore size of the material. The analysis results are calculated according to the BET equation and are presented in Table 2. It is found that the specific surface area of the material gradually increases as the amount of W doped increases, with TiW-0%, TiW-0.5%, TiW-1%, and TiW-1.5% being the values respectively 160.0 m^2/g, 164.6 m^2/g, 168.6 m^2/g and 175.5 m^2/g. This is also consistent with previous XRD and HRTEM results, the material has an anatase structure so the particle size is smaller leading to a larger specific surface area. The surface area of W-doped TiO_2 material is higher than that of other non-carbon supporting materials. The mentioned above can be elucidated by a simple one-step solvothermal process, using inorganic precursors, so the influence of organic macromolecules can be eliminated, as well as not using surface stabilizers or the next stage of heat treatment. This means that the single-step solvothermal method is suitable for nano-size, high crystalline properties, and specific surface area meets the requirements for photocatalytic materials.

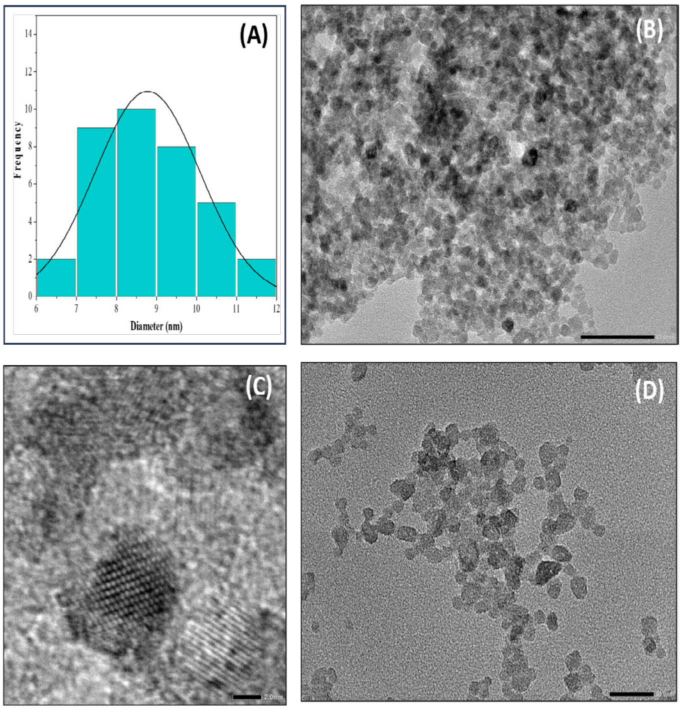

Figure 7: (A) Crystallite size distribution chart of the W-doped TiO_2 catalyst; (B-C-D) HRTEM images of TiO_2.

Table 2: Specific surface area and pore size of catalytic samples.

No.	Samples	Specific surface area S_{BET} (m^2/g)
1	TiW-0%	160.0
2	TiW-0.5%	164.6
3	TiW-1%	168.6
4	TiW-1.5%	175.5

The values of W-doped TiO_2 and other metal doped TiO_2 are briefly listed in Table 3, showing the results of comparisons between this study and other studies. It can be seen that the material synthesized at low temperature is oriented towards the development of the pure anatase structural phase, so the material has a higher specific surface area than the photocatalyst materials of TiO_2 with a mixed phase structure between anatase-rutile-brookite. In addition, the crystallite size of the material is also smaller. These values are probably caused by less agglomeration of composites.

3.2 Results of band gap energy analysis of W-doped TiO_2 nano photocatalyst material

UV-Vis diffuse reflectance spectroscopy method was used to determine the optical properties of W-doped TiO_2 materials. Figure 8a shows the band gap energy of TiO_2 and W-doped TiO_2 catalyst samples with different ratios. The synthesized TiO_2 sample has a band gap energy level at 3.02 eV, lower than anatase TiO_2 of 3.20 eV. The explanation for this may be because the particle size has been significantly reduced when synthesized by the one-stage solvothermal method[52,53]. W-doped TiO_2 samples have a reduced band gap energy compared to TiO_2, specially TiW-0.5%; TiW-1%; TiW-1.5% are 2.96 eV, 2.93 eV and 2.88 eV respectively. This has expanded the visible light absorption region by more than 430 nm (TiW-1.5%) (Figure 8b, 8c). This decrease in band gap energy can be due to the formation of oxygen vacancies, as a result of the doping process. W substitution into the TiO_2 lattice can create many oxygen vacancies, creating a small band below the conduction band of the TiO_2 photocatalyst[54].

Table 3: Surface area, crystallite size and pore size distribution of photocatalysts.

Photocatalysts	Properties				
	Surface area (m^2/g)	**Crystallite size (nm)**	**Pore size (nm)**	**Structure**	**Ref**
TiO_2-EG10	151.4	-	12.3	anatase-rutile	[47]
Cu-doped TiO_2	180-182	7.73-7.86	-	100 wt.% anatase	[48]
2.5 wt.% Fe-doped TiO_2	116.1	7.1-10.3	-	54.1 wt.% anatase, 3.6 wt.% rutile, 42.4 wt.% brookite	[49]
Ni-doped TiO_2	69	25.5-116.7	10.9	$H_2Ti_3O_7$, NiO, TiO_2, brookite	[50]
Ir-doped TiO^2	156-170	10-15	-	anatase-rutile	[51]

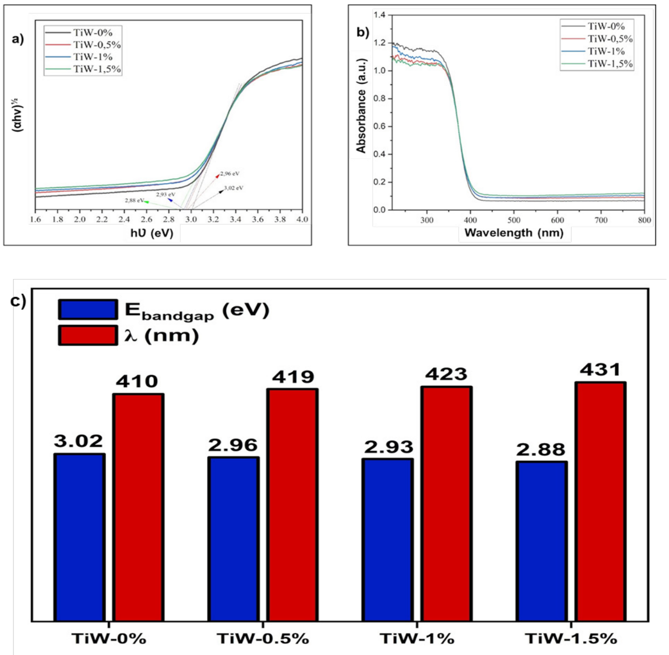

Figure 8: a) Corresponding band gap of TiW-0%, TiW-0.5%, TiW-1% and TiW-1.5% samples, b) UV-Vis diffuse reflectance absorption spectra of TiW-0%, TiW-0.5%, TiW-1% and TiW-1.5% samples, c) Chart of band gap (E_{bg}) and absorbed light wavelength (λ) of catalytic samples.

3.3 Results of investigating the ability of W-doped TiO_2 nanophotocatalytic material to treat formaldehyde

Table 4 and Figure 9 show the formaldehyde concentration in the gas sample before and after going through the gas treatment system and when using a W-doped TiO_2 catalyst with different W ratios and the treatment efficiency of the catalyst samples. Investigation reaction with formaldehyde sample drop volume of 0.05 mL and 0.024 mL of distilled water corresponding to 70% humidity, air flow through the catalyst is 300 mL/min and collected for 10 minutes to fill the bag gas. After the experiment, the air bag was analyzed by gas chromatography analysis to determine formaldehyde concentration. The formaldehyde concentrations in the air bag samples corresponded to the catalyst samples TiW-0%, TiW-0.5%, TiW-1%, and TiW-1.5% respectively 73.0 mg/m³, 63.0 mg/m³, 57.5 mg/m³, 44.0 mg/m³ with formaldehyde removal efficiency of 53.50%, 59.87%, 63.38%, and 71.98%. It can be seen that the formaldehyde decomposition ability of TiW-0% catalytic material is not high. When using a W-doped TiO_2 catalyst, the treatment efficiency increased with the highest TiW-1.5% sample being 71.98%. This may indicate that W doping helps increase the catalytic activity of the material.

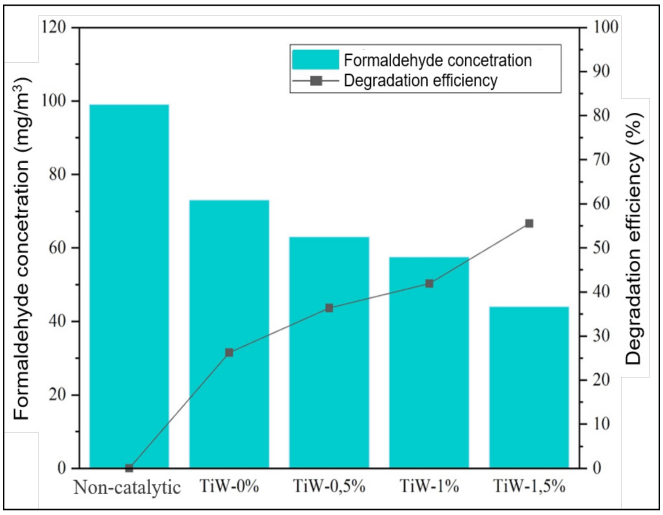

Figure 9: Effect of W doping rate on formaldehyde degradation efficiency.

Table 4: The results of gas chromatography analysis determine the concentration of formaldehyde in gas samples after the experiment.

Catalytic samples	**Volunm of organic droplets (mL)**	**Volunm of H_2O droplets (mL)**	**Air flow (mL/min)**	**Sampling time (min)**	**Formaldehyde concentration (mg/m³)**
-	0.05	0.024	300	10.21	157.0
TiW-0%				10.12	73.0
TiW-0.5%				10.24	63.0
TiW-1%				10.10	57.5
TiW-1.5%				10.32	44.0

Table 5: Preliminary results of surveying the ability to treat formaldehyde using photocatalysts.

Photocatalysts	Initial formaldehyde concentration (mg/m³)	Formaldehyde concentration after reaction C_m (mg/m³)	Processing performance H (%)
TiW-0%	157.0	73.0	53.50
TiW-0.5%		63.0	59.87
TiW-1.0%		57.5	63.38
TiW-1.5%		44.0	71.98

Compared with some previous researches, W-doped TiO2 photocatalyst shows a promising result in treating VOCs degradation (Table 8).

Table 6: The comparison of W-doped TiO_2 photocatalyst with previously studied TiO_2-based materials.

No.	Materials	Synthesize Method	Parameters	Reaction Condition	Object of research	Degradation Efficiency	Reference
1	Co-alloyed TiNbON photocatalyst	Urea-glass synthesize method	- Particle diameter: 1-2m - Surface area: 40.76 m^2/g - Crystalline structure: irregularly shaped surfaces - Band gap: 2.3 eV	- RH: 25-65% - Irradiation: 42-95 (W/m^2) (400-540 nm) - Toluene concentration: 1-5 ppm	Toluene	58%	[55]
3	W-doped TiO_2 photocatalyst	The TiO_2-W nanoparticles was obtained from US Nano Incorporated	- Particle diameter: 10nm - Crystalline structure: Anatase	- T = 30, 40, 60 °C - Photodegradation test: 30 - 180 minutes - Irradiation: UV lamps (10W, 30W, 60W) - Total concentration: 11.21 ppm	Mixture of 4 azo dyes	71%	[56]
4	V-doped TiO_2 / PU (6 wt.%V-TiO_2)	Immobilization of amino titanosiloxane on activated PU combined with utilizing NH_4VO_3 as a precursor	- Surface area: 192.5 m^2/g - Band gap: 2.83 eV for 6 wt.% V-TiO_2	- T = 25 °C - RH= 50% - ARF= 200 mL/min - Irradiation: visible light source with minimum wavelength of 400 nm	Toluene	80%	[22]
5	xAg-Fe co-doped TiO_2 nanoparticles (x = 1, 1.5, 2 mol%)	Sol–Gel Method	- Particle diameter: 10-20nm - Crystalline structure: anatase, brookite - Band gap: 2.93 eV	- Irradiation: visible light (400 – 750nm) - Irradiation time: 0 - 180 minutes - Methylene blue concentration: 5.0 ppm	Methylene Blue	80%	[57]
6	TiO_2/Zeolite (5:95 wt%)	The doping process of titanium dioxide on the zeolite	- Surface area: 53.64 m^2/g - Surface weight: 33.68 mg/cm^2	- Flow rate: 500 – 2000 ml/min - Relative humidity: 35% - Irradiation: UV-C (100–280 nm, 8W) - Toluene concetration: 50ppm	Toluene	70%	[58]
7	W-doped TiO_2 photocatalyst	Solvothermal	- Particle diameter: 6 – 9 nm - Surface area: 175 m^2/g - Crystalline structure: Anatase - Band gap: 2.88 eV	- T = 30 °C - Flow rate: 300 ml/min - Relative humidity: 70% - Irradiation: UV lamp	Formaldehyde	72%	This work

4. Conclusion

In conclusion, we have successfully prepared the novel nanostructured W-doped TiO_2 photocatalyst materials using a one-step, solvothermal method without using any surfactants or a high-temperature calcination phase after the reaction helped reduce the size significantly and increase the specific surface area of the W-doped TiO_2 photocatalytic material, elevating the decomposition efficiency of formaldehyde. The resulting photocatalyst exhibits an anatase phase crystal structure without a WO_3 peak, a spherical morphology, particle size (6 - 10 nm), and enhanced particle distribution. Notably, the TiW-1.5% sample stands out for these attributes. Through BET measurements, surface area analysis revealed the specific surface area of the TiW-1.5% catalyst, surpassing pure TiO_2, with values of 175 m^2/g and 160.0 m^2/g, respectively. Incorporating W ions as W^{6+} into the TiO_2 crystal lattice effectively reduces the band gap energy, particularly evident in the TiW-1.5% catalyst, which displays a reduced band gap energy of 2.88 eV. Our research underscores the potential of W modification in enhancing TiO_2 photocatalytic activity, making it a promising candidate for treating VOCs.

5. References

1. Montero-Montoya R, López-Vargas R, Arellano-Aguilar O. Volatile Organic Compounds in Air: Sources, Distribution, Exposure and Associated Illnesses in Children. Ann Glob Healt 2018;84(2):225-238.
2. Soni V, Singh P, Shree V, Goel V, “Effects of VOCs on Human Health. Air Pollution and Control 2018: pp. 119-142.
3. Gałęzowska G, Chraniuk M, Wolska L. In vitro assays as a tool for determination of VOCs toxic effect on respiratory system: A critical review. TrAC Trends in Analytical Chemistry 2015;77:14-22.
4. Padhi SK, Gokhale S.Treatment of gaseous volatile organic compounds using a rotating biological filter. Bioresour Technol 2017;244:270-280.
5. Wang F, Lei X, Hao H. Key factors in the volatile organic compounds treatment by regenerative thermal oxidizer. J Air Waste Manag Assoc 2020;70(5):557-567.
6. Kamal MS, Razzak SA, Hossain MM. Catalytic oxidation of volatile organic compounds (VOCs) – A review. *Atmospheric Environment 2016;140*:117-134.
7. Li X, Zhang L, Yang Z, *et al.* Hydrophobic modified activated carbon using PDMS for the adsorption of VOCs in humid condition. *Separation and Purification Technology 2020;*239:116517.
8. Kim JM, Kim JH, Lee CY, Jerng DW, Ahn HS. Toluene and acetaldehyde removal from air on to graphene-based adsorbents with microsized pores. *J Hazard Mater 2018;344:458-465.*
9. Hariz R, Rio Sanz JID, Mercier C, *et al.* Absorption of toluene by vegetable oil–water emulsion in scrubbing tower: Experiments and modeling. *Chemical Engineering Science 2016;157:*264-271.
10. Laskar II, Hashisho Z, Phillips JH, Anderson JE, Nichols M. Competitive adsorption equilibrium modeling of volatile organic compound (VOC) and water vapor onto activated carbon. *Separation and Purification Technology 2019;212:* 632-640.

11. Takeuchi M, Hidaka M, Anpo M. Efficient removal of toluene and benzene in gas phase by the TiO2/Y-zeolite hybrid photocatalyst. *J Hazard Mater 2012;* 237-238:133-139.

12. Šuligoj A, Štangar UL, Ristić A, Mazaj M, Verhovšek D, Tušar NN. TiO2–SiO2 films from organic-free colloidal TiO2 anatase nanoparticles as photocatalyst for removal of volatile organic compounds from indoor air. *Applied Catalysis B: Environmental 2016;*184:119-131.

13. Li R, Li T, Zhou Q. Impact of Titanium Dioxide (TiO2) Modification on Its Application to Pollution Treatment—A Review. *Catalysts 2020*;10(7):804.

14. Liao Y, Que W, Jia Q, He Y, Zhang J, Zhong P. Controllable synthesis of brookite/anatase/rutile TiO 2 nanocomposites and single-crystalline rutile nanorods array. *Journal of Materials Chemistry 2012;*22(16):7937-7944.

15. Gupta SM, Tripathi M. A review of TiO2 nanoparticles. *Chinese Science Bulletin 2011;56:*1639-1657.

16. Zhang J, Zhou P, Liu J, Yu J. New understanding of the difference of photocatalytic activity among anatase, rutile and brookite TiO2. Physical Chemistry Chemical Physics 2014; 16(38):20382-20386.

17. Eddy DR, Permana MD, Sakti LK, *et al.* Heterophase Polymorph of TiO2 (Anatase, Rutile, Brookite, TiO2 (B)) for Efficient Photocatalyst: Fabrication and Activity. *Nanomaterials 2023;13(4):*704.

18. Dong H, Zeng G, Tang L, *et al*. An overview on limitations of TiO2-based particles for photocatalytic degradation of organic pollutants and the corresponding countermeasures. *Water Research 2015;79:*128-146.

19. Liang W, Li J, Jin Y. Photo-catalytic degradation of gaseous formaldehyde by TiO2/UV, Ag/TiO2/UV and Ce/TiO2/UV. *Building and Environment 2012;51:*345-350.

20. Li Y, Zhang C, Ma J, Chen M, Deng H, He H, High temperature reduction dramatically promotes Pd/TiO2 catalyst for ambient formaldehyde oxidation. *Applied Catalysis B: Environmental;*217:560-569.

21. Duan B, Zhou Y, Huang C, *et al*. Impact of Zr-Doped TiO2 Photocatalyst on Formaldehyde Degradation by Na Addition. Ind. Eng. Chem 2018;57(42):14044-14051

22. Pham TD, Lee BK. Novel adsorption and photocatalytic oxidation for removal of gaseous toluene by V-doped TiO2/PU under visible light. Journal of Hazardous Materials 2015;300:493-503.

23. Laokiat L, Khemthong P, Grisdanurak N, Sreearunothai P, Pattanasiriwisawa W, Klysubun W. Photocatalytic degradation of benzene, toluene, ethylbenzene, and xylene (BTEX) using transition metal-doped titanium dioxide immobilized on fiberglass cloth. *Korean Journal of Chemical Engineering 2012;*29:377-383.

24. Carvalho HWP, Rocha MVJ, Hammer P, Ramalho TC. TiO2–Cu photocatalysts: a study on the long- and short-range chemical environment of the dopant. *Journal of Materials Science 2013;*48(11):3904-3912.

25. Stucchi M, Bianchi CL, Carlo P, *et al.* Copper NPs decorated titania: A novel synthesis by high energy US with a study of the photocatalytic activity under visible light. *Ultrasonics Sonochemistry 2016;*31:295-301.

26. Moradi V, Jun BGM, Blackburn AM, Herring RA. Significant improvement in visible light photocatalytic activity of Fe doped TiO2 using an acid treatment process. *Applied Surface Science 2017;*427:791-799.

27. Feng F, Yang W, Gao S, Sun C, Li Q. Postillumination Activity in a Single-Phase Photocatalyst of Mo-Doped TiO2 Nanotube Array from Its Photocatalytic "Memory". ACS Sustainable Chemistry & Engineering 2018;6(5):6166-6174.

28. Shu Y, Ji J, Xu Y, *et al.* Promotional role of Mn doping on catalytic oxidation of VOCs over mesoporous TiO2 under vacuum ultraviolet (VUV) irradiation. *Applied Catalysis B: Environmental 2018;*220:78-87.

29. Tsang CHA, Li K, Zeng Y, *et al.* Titanium oxide based photocatalytic materials development and their role of in the air pollutants degradation: Overview and forecast. Environ Int 2019;125: 200-228

30. Priya VS, Philip L. Photocatalytic Degradation of Aqueous VOCs Using N Doped TiO2: Comparison of Photocatalytic Degradation under Visible and Sunlight Irradiation. *International Journal of Environmental Science and Development 2015;*6(4):286-291

31. Guo D, Feng D, Zhang Y, *et al.* Carbon material-TiO2 for photocatalytic reduction of CO2 and degradation of VOCs: A critical review. *Fuel Processing Technology 2022;*231:107261.

32. Zhang J, Hu Y, Qin J, Yang Z, Fu M. TiO2-UiO-66-NH2 nanocomposites as efficient photocatalysts for the oxidation of VOCs. Chemical Engineering Journal 2020;385:123814

33. Lyu J, Zhou L, Shao J, *et al.* Synthesis of TiO2/H2Ti3O7 composite with nanoscale spiny hollow hierarchical structure for photocatalytic mineralization of VOCs. *Chemical Engineering Journal 2020;*400:125927.

34. Li JJ, Cai SC, Yu EQ, *et al.* Efficient infrared light promoted degradation of volatile organic compounds over photo-thermal responsive Pt-rGO-TiO2 composites. *Applied Catalysis B: Environmental 2018;*233:260-271.

35. Akhter P, Arshad A, Saleem A, Hussain M, Recent Development in Non-Metal-Doped Titanium Dioxide Photocatalysts for Different Dyes Degradation and the Study of Their Strategic Factors: A Review. Catalysts 2022;12(11):1331.

36. Poorkarimi A, Karimi-Jashni A, Javadpour S. Optimization of toluene removal over W-doped TiO2 nano-photocatalyst under visible light irradiation. *Environmental Technology 2018;*39(24) 3135-3148.

37. Oseghe EO, Ndungu PG, Jonnalagadda SB. Photocatalytic degradation of 4-chloro-2-methylphenoxyacetic acid using W-doped TiO2. *Journal of Photochemistry and Photobiology A: Chemistry 2015;*312:96-106.

38. Kapilashrami M, Zhang Y, Liu YS, Hagfeldt A, Guo J. Probing the optical property and electronic structure of TiO2 nanomaterials for renewable energy applications. *Chem. Rev 2014;114(19)* 9662-9707.

39. Teh CM, Mohamed AR. Roles of titanium dioxide and ion-doped titanium dioxide on photocatalytic degradation of organic pollutants (phenolic compounds and dyes) in aqueous solutions: A review. *Journal of Alloys and Compounds 2011;*509(5):1648-1660.

40. Filippatos PP, Kelaidis N, Vasilopoulou M, Davazoglou D, Chroneos A. Structural, Electronic, and Optical Properties of Group 6 Doped Anatase TiO2: A Theoretical Approach. Appl. Sci. 2021;11(4):1657.

41. Santos E, Catto AC, Peterline AF, Avansi Jr W. Transition metal (Nb and W) doped TiO2 nanostructures: The role of metal doping in their photocatalytic activity and ozone gas-sensing performance. *Applied Surface Science 2022;*579:152146.

42. Pham HQ, Huynh TT, Nguyen AV, Thuan TV, Bach LG, Ho VTT. Advanced Ti(0.7)W(0.3)O_2 Nanoparticles Prepared via Solvothermal Process Using Titanium Tetrachloride and Tungsten Hexachloride as Precursors. *J Nanosci Nanotechnol 2018;18(10):*7177-7182.

43. Huynh TT, Pham HQ, Nguyen AV *et al.* High conductivity and surface area of Ti0.7W0.3O2 mesoporous nanostructures support for Pt toward enhanced methanol oxidation in DMFCs. *International Journal of Hydrogen Energy 2019;44(37):*20933-20943.

44. H. D. Goodfellow HD, and E. F. Curd, “Chapter 4 - Physical fundamentals,” in *Industrial Ventilation Design Guidebook (Second Edition)*. Academic Press 2020:39-109.

45. Pham HQ, Huynh TT, Bach LG, Ho VTT. Synthesis and characterization the multifunctional nanostructures TixW1-xO2 (x = 0.5; 0.6; 0.7; 0.8) supports as robust non-carbon support for Pt nanoparticles for direct ethanol fuel cells. *International Journal of Hydrogen Energy 2021;46(48):*24877-24890

46. Gao L, Zhang Q. Effects of amorphous contents and particle size on the photocatalytic properties of TiO2 nanoparticles. *Scripta Materialia 2001;44(8)*: 1195-1198.

47. Xiong J, Zhang M, Cheng G. Facile polyol-triggered anatase–rutile heterophase TiO2-x nanoparticles for enhancing photocatalytic CO2 reduction. *Journal of Colloid and Interface Science 2020;579:*872-877.

48. Mingmongkol Y, Trinh DTT, Phuinthiang P, *et al.* Enhanced Photocatalytic and Photokilling Activities of Cu-Doped TiO2 Nanoparticles. *Nanomaterials 2022; 12(7)*,1198.

49. Mancuso A, Blangetti N, Sacco O, *et al.* Photocatalytic Degradation of Crystal Violet Dye under Visible Light by Fe-Doped TiO2 Prepared by Reverse-Micelle Sol–Gel Method. *Nanomaterials 2023;*13(2):270.

50. Shaban M, Ahmed AM, Shehata N, Betiha MA, Rabie MR. Ni-doped and Ni/Cr co-doped TiO2 nanotubes for enhancement of photocatalytic degradation of methylene blue. *Journal of Colloid and Interface Science 2019;*555:31-41.

51. Ho VTT, Chau DH, Bui KQ, *et al.* A High-Performing Nanostructured Ir Doped-TiO2 for Efficient Photocatalytic Degradation of Gaseous Toluene. *Inorganics* 2022;10(3):10030029.

52. Jung KY, Park SB, Effect of calcination temperature and addition of silica, zirconia, alumina on the photocatalytic activity of titania. *Korean Journal of Chemical Engineering 2001;18(6):*879-888.

53. Maira AJ, Yeung KL, Lee CY, Yue PL, Chan CK. Size Effects in Gas-Phase Photo-oxidation of Trichloroethylene Using Nanometer-Sized TiO2 Catalysts. *Journal of Catalysis 2000;192(1):*185-196.

54. Ho VTT, Chau DH, Bui KQ, *et al.* A High-Performing Nanostructured Ir Doped-TiO2 for Efficient Photocatalytic Degradation of Gaseous Toluene. *Inorganics* 2022;10(3):10030029.

55. Zhong L, Brancho LL, Batterman S, Bartlett BM, Godwin C. Experimental and modeling study of visible light responsive photocatalytic oxidation (PCO) materials for toluene degradation. Appl Catal B 2017;216:122-132.

56. Effiong JF, Nyong AE, Obadimu C, Udoh G. Photocatalytic degradation and kinetics of dyes in textile effluent using uv-tio2-w system. J. Mater. Environ. Sci 2023; 14(8):946, 2023.

57. Sukhadeve GK, Bandewar H, Janbandhu SY, Jayaramaiah JR, Gedam RS. Photocatalytic hydrogen production, dye degradation, and antimicrobial activity by Ag-Fe co-doped TiO2 nanoparticles, *Journal of Molecular Liquids 2023;369*:120948.

58. Rangkooy HA, Mokaramian S, Zargar B. Photocatalytic Removal of Toluene Vapour Pollutant from the Air Using Titanium Dioxide Nanoparticles Supported on the Natural Zeolite. *Iran J Public Health 2023;52(1)*184-192.